EPJ Web of Conferences **346**, 01024 (2026) https://doi.org/10.1051/epjconf/202634601024
RFPPC2025

Studies of various lower hybrid wave launch scenarios for non-inductive start-up on TST-2

Naoto Tsujii[1,*], *Fumiya* Adachi[1], *Akira* Ejiri[1], *Kouji* Shinohara[1], *Yi* Peng[1], *Yuting* Lin[1], *Zhengnan* Jiang[1], *Yiming* Tian[1], *Yangguang* Jiang[1], *Shengyu* Wang[1], *Masaru* Yoshida[1], and *Yuta* Takechi[1]

[1]The University of Tokyo, Kashiwa, Chiba 277-8561, Japan

Abstract. Efficient non-inductive start-up of a spherical tokamak may be achieved by using lower hybrid waves that have high current drive efficiency. On the TST-2 spherical tokamak, three lower hybrid launchers are installed at the outer-midplane, top and outer-off-midplane to explore efficient start-up scenarios. The previously installed outer-midplane and top launchers were both found to drive current far off-axis where confinement of fast electrons were expected to be low. The outer-off-midplane launcher was newly developed to increase current drive by improving absorption closer to the magnetic axis. The outer-off-midplane launcher driven plasma was confirmed to have higher core electron temperature than those of the previous two launchers, and reduced fast electron losses compared to the top launcher.

1 Introduction

Establishment of a non-inductive start-up method will make a large central solenoid (CS) unnecessary, which may lead to an economical spherical tokamak fusion reactor. Radio frequency (RF) waves are widely used to heat a plasma as well as drive current. Non-inductive start-up using rf waves has been studied for electron cyclotron waves [1–3] and lower hybrid waves [4–6]. Lower hybrid start-up has an advantage of having a high current drive efficiency at the low temperature of the initial plasma. CS-less formation of advanced tokamak has been demonstrated on JT-60U by utilizing lower hybrid waves [7].

On TST-2, fully non-inductive plasma current ramp-up up to 26 kA, which is about a quarter of the ohmically driven value, has been achieved using the outer-midplane and top lower hybrid launchers [8, 9]. Numerical analysis showed that the current was driven far off-axis for these two scenarios that limited the driven current. The outer-off-midplane launcher was newly developed to drive current closer to the magnetic axis [10]. The core electron temperature of the (outer-)off-midplane launcher driven discharge was found to be substantially higher than those of outer-midplane and top launcher driven discharges, confirming qualitatively the improved core absorption of the new scenario.

In this paper, we report our progress in the understanding of the current drive characteristics of the three launch scenarios. Numerical analysis was performed using the ray tracing code GENRAY [11] and the Fokker-Planck code CQL3D [12].

*Corresponding author: tsujii@k.u-tokyo.ac.jp

Table 1. The nominal parameters of the three lower hybrid launchers. R, Z are the coordinates of the strap surface midpoint and $N_{\|}$ is the peak toroidal refractive index.

	R [m]	Z [m]	$N_{\|}$
Outer-midplane	0.621	0	5.5
Top	0.283	0.436	4.9
Off-midplane	0.595	0.179	13

2 Experimental setup

TST-2 is a spherical tokamak located at the University of Tokyo ($R_0 = 0.36$ m, $a = 0.23$ m, $B_{t0} < 0.3$ T). Three lower hybrid launchers are operated at 200.1 MHz. The source power is 100 kW for each launcher. The outer-midplane launcher [9], the top launcher [8] and the (outer-)off-midplane launcher [10] are presently installed. The parameters of the lower hybrid launchers are shown in table 1. Electron cyclotron heating at 2.45 GHz was applied to assist breakdown, and was turned off for the rest of the discharge.

3 The outer-midplane launcher driven plasma

Figure 1 shows the trajectories of lower hybrid waves launched from the outer-midplane antenna for the discharge shown in figure 11 and 12 of ref. [4]. The phase space trajectories of the same rays are shown in figure 2(a). The hatched region shows the inaccessible parameter space. The high phase velocity limit is given by the mode conversion limit. The low phase velocity limit is given by the absorption limit that is three times the bulk electron thermal velocity. The lower hybrid start-up

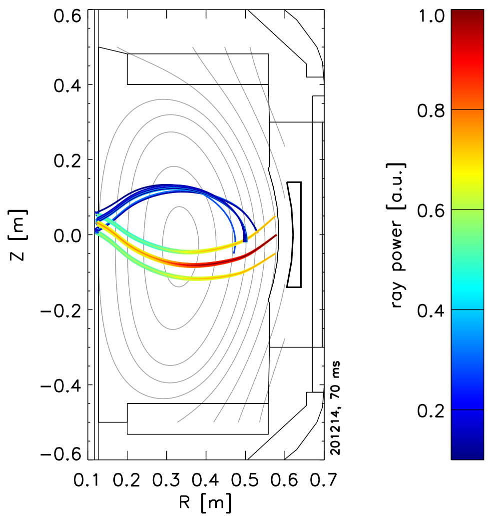

Figure 1. The typical lower hybrid ray trajectories for the outer-midplane launcher.

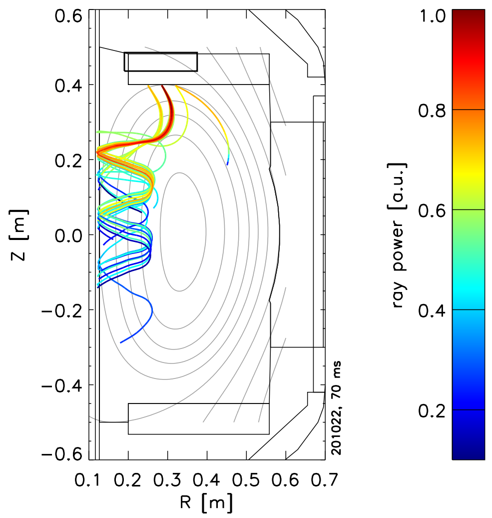

Figure 3. The typical lower hybrid ray trajectories for the top launcher.

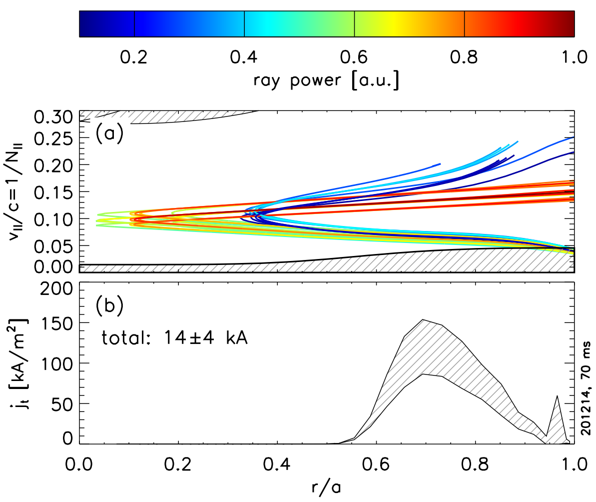

Figure 2. (a) The phase space ray trajectory for the outer-midplane launcher. The hatched region shows the inaccessible parameter space. (b) The simulated driven current profile for the outer-midplane launcher. The density profile was perturbed within experimental errorbars to estimate the uncertainty of the prediction.

plasma on TST-2 typically have electron temperature of 5–40 eV depending on the condition [4]. Parallel refractive index of at least $N_\parallel \sim 27$ is required for good absorption in this cold initial start-up plasma. For the outer-midplane launch scenario, this is achieved through up-shift of the toroidal index of refraction. The waves are launched at central $N_\parallel$ of $\sim$5.5 and up-shifts to $N_\parallel \sim 26$ at the inner limiter ($R = 0.13$ m). Consistently with the expected absorption mechanism that is purely geometrical (i.e., $1/R$ up-shift of the toroidal refractive index), the outer-midplane launch scenario has a relatively robust current drive characteristics for plasma current of zero up to $\sim$20 kA.

The predicted driven current profile is shown in figure 2(b). The driven current is not limited by the available power, but by complete flattening of the parallel velocity distribution [13]. Since the current density is already saturated, higher density is required for electrons to carry more current, but this pushes the absorption region more outward, deteriorating the total driven current. Experimentally, the maximum plasma current has been limited to 21 kA for the outer-midplane launch scenario under the present configuration of TST-2 [14].

4 The top launcher driven plasma

Figure 3 shows the trajectories of lower hybrid waves launched from the top antenna for the discharge shown in figure 11 and 12 of ref. [4]. The phase space trajectories of the same rays are shown in figure 4(a). The waves are launched at somewhat lower $N_\parallel$ compared to the outer-midplane launcher, but because of the smaller major radius, the minimum of the $N_\parallel$ spectrum in the plasma is actually less than a half of the outer-midplane launcher. Good absorption is achieved with the top launch scenario, however, thanks to strong poloidal up-shift of $N_\parallel$. This mechanism allows for broad wavenumber spectrum to be generated for the top launch scenario, which is suited to accelerate cold (and slow) electrons to very high parallel velocity, achieving high current density. Since the absorption mechanism of the top launch scenario relies on the existence of plasma, it can not efficiently start plasma current from zero. Usually, on TST-2, the plasma is started-up with the outer-midplane launcher up to $\sim$10 kA and switched over to the top launcher to ramp-up the plasma current further. As long as the density is sufficiently high, $N_\parallel$ is predicted to up-shift until the waves are absorbed, resulting in good absorption. Operating at lower density has been easier for the top launcher compared to the outer-midplane launcher, suggesting that the absorption is in-

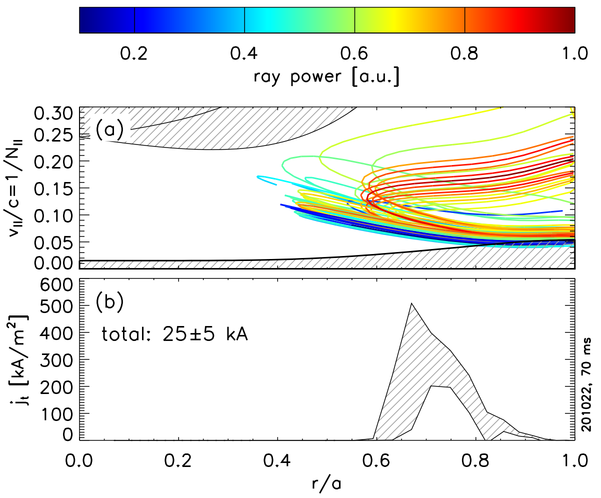

Figure 4. (a) The phase space ray trajectory for the top launcher. The hatched region shows the inaccessible parameter space. (b) The simulated driven current profile for the top launcher. The density profile was perturbed within experimental errorbars to estimate the uncertainty of the prediction.

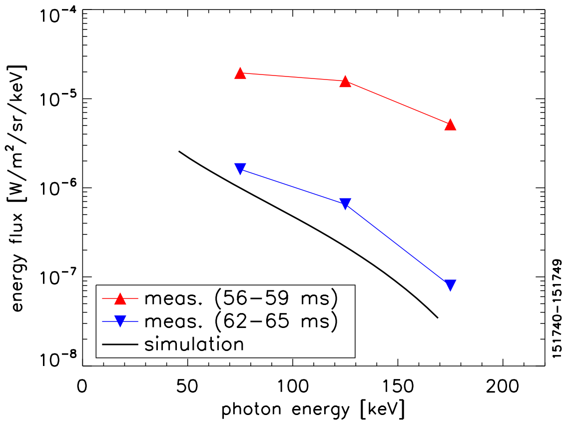

Figure 5. The measured and simulated hard x-ray energy spectrum for the top launcher. Radial view at $Z = -0.200$ m. Red upward triangle: measured energy flux during the power-on phase (56–59 ms); blue downward triangles: measured energy flux during the power-off phase (62–65 ms); black solid curve: simulated core radiation.

deed good and the wave interactions with the wall is reduced.

The predicted driven current profile is shown in figure 4(b). The current density is higher than the outer-midplane launch case, resulting in greater total driven plasma current. The absorption region, however, is still limited to far off-axis due to strong refraction the waves experience for this scenario. Current density is saturated similarly to the outer-midplane launch case. Experimentally, the maximum plasma current has been limited to 26 kA for the top launcher [14]. This is the maximum non-inductive plasma current achieved on TST-2 so far.

Figure 5 shows comparison of the measured and simulated x-ray energy spectrum. It can be seen that the measured x-ray radiation intensity during the power-on phase is about an order of magnitude greater than the simulation that only accounts for radiation from the core. Figure 6 shows the time evolution of the hard x-ray radiation during lower hybrid power modulation. Simulation predicts negligible change of the radiation intensity during this time window due to the long slowing down time of the core fast electrons. However, the measurement shows prompt drop of the x-ray radiation intensity within 1 ms. This suggests that the x-ray radiation observed during the power-on phase is not coming from the core, but coming from the thick-target radiation of fast electrons lost at the limiters. Indeed, figure 5 shows that the x-ray energy spectrum shortly after power-off is consistent with the simulated fast electron radiation from the core. The observed prompt reduction of the x-ray radiation suggests that the fast electron loss is likely driven by the waves themselves through the finite orbit effect [15]. The x-ray radiation during the power-on phase is much higher for the top launcher compared to the outer-midplane launcher [4], which indi-

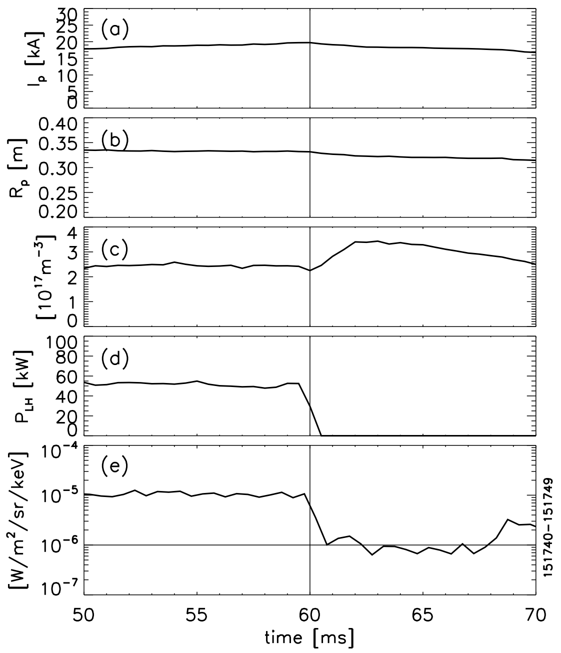

Figure 6. The time evolution of the measured and simulated hard x-ray radiation intensity for the top launcher. The vertical lines at 60 ms indicates the rf power-off timing. (a) Plasma current (b) major radius of plasma center (c) line-averaged electron density (d) lower hybrid power (e) hard x-ray radiation intensity (50–100 keV). The horizontal line shows the simulated core radiation.

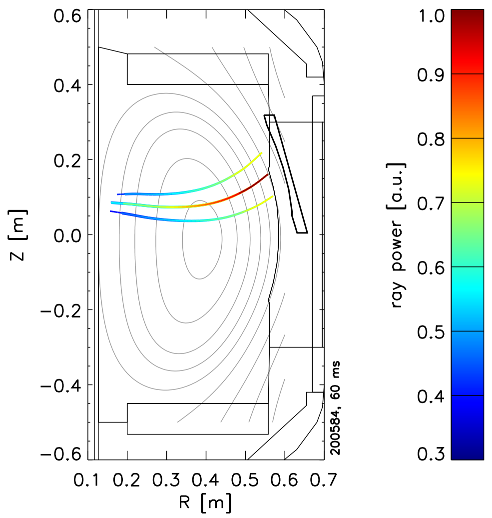

Figure 7. The typical lower hybrid ray trajectories for the off-midplane launcher.

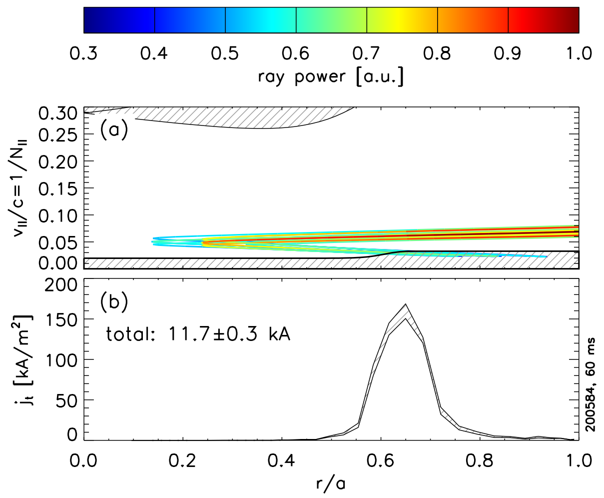

Figure 8. (a) The phase space ray trajectory for the off-midplane launcher. The hatched region shows the inaccessible parameter space. (b) The simulated driven current profile for the off-midplane launcher. The density profile was perturbed within experimental errorbars to estimate the uncertainty of the prediction.

cates that not only the fast electron energy but also such orbit losses are much greater for the top launch scenario.

The agreement of the simulated driven current with the experiment is remarkable considering the fact that it does not take into account the finite orbit effect which seems to be substantial experimentally. The possible reason is that the parallel velocity distribution is saturated at the present parameters. Since the current density is already saturated, it is not sensitive to small differences in the model as far as the current drive location is adequately simulated. This suggests that scenarios that can deposit power closer to the magnetic axis is needed to drive more current.

5 The off-midplane launcher driven plasma

To overcome the limit of the outer-midplane and the top launchers, the off-midplane launcher was newly developed. The scenario was designed to drive current closer to the magnetic axis. Figure 7 shows the typical trajectories of lower hybrid waves launched from the off-midplane antenna for the plasma generated in the actual experiment presented in figure 2 and 3 of ref. [4]. The ray paths were shifted upwards compared to the design target [16] due to the lower plasma current. The phase space trajectories of the same rays are shown in figure 8(a). Good absorption is expected closer to the axis. The temperature was found to be substantially higher for the off-midplane launcher generated plasma compared to the previous two launchers [4, 10]. On the other hand, the driven current fell short of expectations, at 8 kA [4]. Figure 8(b) shows the predicted driven current density. The simulated total plasma current was much smaller than our design target. This was due to the lower plasma current, lower density and lower power. The power was limited due to frequent arcing at the antenna. We have modified the limiter to increase the distance of the straps to the plasma. So far, we were able

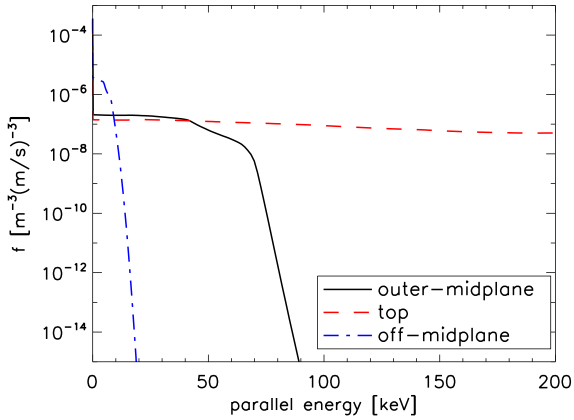

Figure 9. The simulated parallel distribution function at the current peak for the outer-midplane (r/a = 0.69), top (r/a = 0.69) and off-midplane (r/a = 0.65) launch scenarios.

to increase the coupled power by 50 % (to 40 kW) and observed modest plasma current increase of about 10 % . We aim to increase the coupled power further by a factor of four.

The discrepancy between the simulated and measured total plasma current was found to be more significant for the off-midplane launch scenario compared to the previous two scenarios. The simulated distribution function for the off-midplane launch scenario is plotted with those for the outer-midplane and top launch scenarios in figure 9. The maximum energy for the outer-midplane and top launch scenarios are determined by the accessibility limit at the low-field side and high-field side, respectively. In contrast, the tail of the off-midplane launch scenario has much lower energy. Figure 10 shows the power dependence of

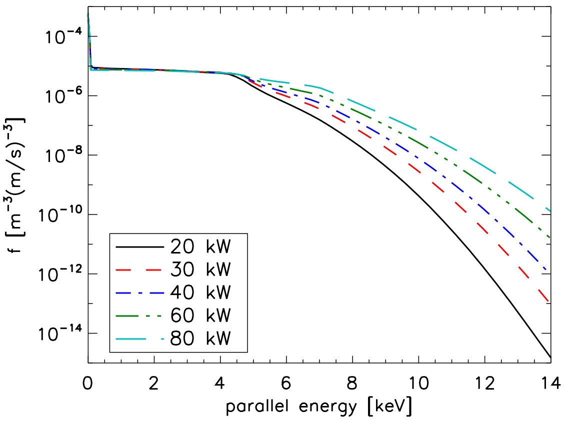

Figure 10. The simulated parallel distribution function at the current peak (r/a = 0.65) for the off-midplane launch scenario. The plateau extended with the incident lower hybrid power.

the distribution function for the off-midplane launch case. It can be seen that the current density is not saturated for the present off-midplane launch case, and it is possible that the zero orbit model is not accurate enough for quantitative prediction.

6 Conclusions

Three lower hybrid start-up scenarios have been studied on the TST-2 spherical tokamak. Fully non-inductive lower hybrid start-up was demonstrated with the outer-midplane launcher. In the outer-midplane launch scenario, the absorption was achieved through up-shift of the toroidal index of refraction, allowing for plasma current ramp-up from zero. The top launch scenario could generate broad wavenumber spectrum suited for current drive through poloidal refractive index up-shift. However, strong refraction limited the absorption region to far off-axis. The off-midplane launch scenario was designed to drive current closer to the magnetic axis and overcome the limit of the previous two launchers. So far, the plasma current driven by the off-midplane launcher remained lower than the previous two launchers due to limited coupled power to the plasma. Increase of lower hybrid power at higher plasma density may be necessary for the off-midplane launcher to overcome the plasma current achieved by the previous two launchers.

7 Acknowledgements

The authors thank R.W. Harvey for providing the GENRAY and CQL3D codes. This work was supported by JSPS KAKENHI Grant Numbers 22K03573, 18K13524 and 21226021, NIFS Collaboration Research Programs NIFS18KOAR22 and NIFS20KUTR155 and Japan/US Cooperation in Fusion Research and Development.

References

[1] H. Tanaka, M. Uchida, T. Maekawa, Y.S. Bae, M. Joung, J. Jeong, K. team, Non-inductive initiation of closed flux surfaces by ECH/ECCD on KSTAR using an oblique fundamental O-mode injection from the low-field side, Nuclear Fusion **56**, 046003 (2016). https://doi.org/10.1088/0029-5515/56/4/046003

[2] M. Uchida, T. Yoshinaga, H. Tanaka, T. Maekawa, Rapid current ramp-up by cyclotron-driving electrons beyond runaway velocity, Phys. Rev. Lett. **104**, 065001 (2010). https://doi.org/10.1103/PhysRevLett.104.065001

[3] C.B. Forest, Y.S. Hwang, M. Ono, D.S. Darrow, Internally generated currents in a small-aspect-ratio tokamak geometry, Phys. Rev. Lett. **68**, 3559 (1992). https://doi.org/10.1103/PhysRevLett.68.3559

[4] N. Tsujii, A. Ejiri, Y. Ko, Y. Peng, K. Iwasaki, Y. Lin, K. Shinohara, O. Watanabe, S. Jang, T. Hidano et al., Studies of the outer-off-midplane lower hybrid wave launch scenario for plasma start-up on the TST-2 spherical tokamak, Nuclear Fusion **64**, 086017 (2024). https://doi.org/10.1088/1741-4326/ad52a9

[5] V. D'yachenko, V. Gusev, M. Larionov, A. Mel'nik, A. Novokhatskii, Y. Petrov, V. Rozhdestvenskii, N. Sakharov, A. Stepanov, S. Khitrov et al., Noninductive plasma generation and current drive in the Globus-M spherical tokamak, Plasma Physics Reports **39**, 189 (2013). https://doi.org/10.1134/S1063780X1303001X

[6] K. Toi, K. Ohkubo, K. Kawahata, Y. Kawasumi, K. Matsuoka, N. Noda, Y. Ogawa, K. Sato, S. Tanahashi, T. Tetsuka et al., Startup and quasistationary drive of plasma current by lower hybrid waves in a tokamak, Phys. Rev. Lett. **52**, 2144 (1984). https://doi.org/10.1103/PhysRevLett.52.2144

[7] S. Shiraiwa, S. Ide, S. Itoh, O. Mitarai, O. Naito, T. Ozeki, Y. Sakamoto, T. Suzuki, Y. Takase, S. Tanaka et al. (JT-60 Team), Formation of advanced tokamak plasmas without the use of an ohmic-heating solenoid, Phys. Rev. Lett. **92**, 035001 (2004). https://doi.org/10.1103/PhysRevLett.92.035001

[8] S. Yajima, Y. Takase, Y. Tajiri, Y. Takei, N. Tsujii, H. Yamazaki, C. Moeller, T. Shinya, Development of capacitively-coupled combline antennas for current drive in tokamaks, Nuclear Fusion **59**, 066004 (2019). https://doi.org/10.1088/1741-4326/ab0f61

[9] T. Shinya, Y. Takase, S. Yajima, C. Moeller, H. Yamazaki, N. Tsujii, Y. Yoshida, A. Ejiri, H. Togashi, K. Toida et al., Plasma current start-up experiments using outboard- and top-launch lower hybrid wave on the TST-2 spherical tokamak, Nuclear Fusion **57**, 036006 (2016). https://doi.org/10.1088/1741-4326/57/3/036006

[10] Y. Ko, N. Tsujii, A. Ejiri, O. Watanabe, S. Jang, K. Shinohara, K. Iwasaki, Y. Peng, Y. Lin, Y. Shirasawa et al., Development of an outer-off-midplane lower hybrid wave launcher for im-

proved core absorption in non-inductive plasma start-up on TST-2, Nuclear Fusion **63**, 126015 (2023). https://doi.org/10.1088/1741-4326/acf5ff

[11] A. Smirnov, R. Harvey, A general ray tracing code GENRAY, Bull. Am. Phys. Soc. **39**, 1626 (1994).

[12] R.W. Harvey, M.G. McCoy, CQL3D Fokker-Planck code, Proceedings of the IAEA Technical Committee Meeting on Simulation and Modeling of Thermonuclear Plasmas, Montreal, Canada, 1992 (USDOC NTIS Document No. DE93002962) p. 40, eDB/700350 (1992).

[13] N. Tsujii, Y. Takase, A. Ejiri, T. Shinya, H. Togashi, S. Yajima, H. Yamazaki, C. Moeller, B. Roidl, M. Sonehara et al., Numerical modeling of lower hybrid current drive in fully non-inductive plasma start-up experiments on TST-2, Nuclear Fusion **57**, 126032 (2017). https://doi.org/10.1088/1741-4326/aa8568

[14] S. Yajima, Y. Takase, A. Ejiri, N. Tsujii, H. Yamazaki, C.P. Moeller, T. Shinya, Y. Takei, Y. Tajiri, Y. Yoshida et al., Current drive experiment using top/outboard side lower hybrid wave injection on TST-2 spherical tokamak, Plasma and Fusion Research **13**, 3402114 (2018). https://doi.org/10.1585/pfr.13.3402114

[15] A. Ejiri, H. Yamazaki, Y. Takase, N. Tsujii, O. Watanabe, Y. Peng, K. Iwasaki, Y. Aoi, Y. Ko, K. Matsuzaki et al., A fast electron transport model for lower hybrid wave sustained plasmas, Plasma and Fusion Research **17**, 1402037 (2022). https://doi.org/10.1585/pfr.17.1402037

[16] Y. Ko, N. Tsujii, A. Ejiri, O. Watanabe, K. Shinohara, Y. Peng, K. Iwasaki, Y. Lin, G. Yatomi, I. Yamada et al., Development of an off-midplane launch lower hybrid antenna for improved core current drive in non-inductive start-up plasmas on TST-2, AIP Conference Proceedings **2984**, 090001 (2023), https://doi.org/10.1063/5.0162483